Horizontal Biaxial Loading Tests on Sliding Lead Rubber Bearing System

M. Yamamoto, H. Hamaguchi & N. Kamoshita

Takenaka Research and Development Institute, Japan.

M. Kikuchi & K. Ishii

Hokkaido University, Japan.

T. Wake

Oiles Corporation, Japan.

2017 NZSEE Conference

ABSTRACT: The authors have proposed a high-safety-margin seismic isolation system for large earthquakes that exceed design basis earthquakes (DBE). This system consists of a lead rubber bearing (LRB) and a sliding bearing in series. The system functions as a conventional LRB under earthquakes smaller than DBE; under those larger than DBE, the sliding bearing slides and prevents the failure of the LRB. Dynamic loading tests of the system were conducted. The target size of the LRB in the system was 900 × 900 mm. The test specimens, reduced 4.5 times in length from the original size, measured 200 × 200 mm. Horizontal displacements were applied under various axial force conditions with constant average stresses of 4, 8, and 12 MPa. A displacement-dependent case was studied with average stress varying between 4 and 12 MPa. The horizontal loadings were applied uniaxially and biaxially as circles and ellipses. Test results showed that the previously reported design equation of friction force was applicable for both biaxial and uniaxial loadings. However, biaxial loading caused torsional deformation in the LRB, which increased the shear strain relative to that under corresponding uniaxial loading. The system was analytically modelled and implemented in OpenSees software. This analytical model simulated the test results precisely for various frequencies, various axial forces, and both uniaxial and biaxial horizontal loadings.

1 INTRODUCTION

Recently, damage of building structures under unexpected large earthquakes has become apparent. Behaviours of seismically isolated (SI) buildings under large earthquakes that exceed design basis earthquakes (DBE) have been studied. The authors have proposed and studied a seismic isolator system with a high safety margin for large earthquakes exceeding DBE. The system comprises a lead rubber bearing (LRB) and a sliding bearing connected in series (Hamaguchi et al. 2010).

Horizontal bidirectional characteristics are also a growing concern in seismic isolation. Experimental studies on LRB (Nakamura et al. 2012) and elastic sliding bearings (Yamamoto et al. 2012a; Kamoshita et al. 2014) have been conducted. These studies revealed that the restoring force of the bearing was highly affected by horizontal bidirectional loading, while the shear strain of a rubber bearing was increased by torsional deformation induced by bidirectional loading. The proposed isolation system was also affected by horizontal bidirectional loading. Hence, dynamic loading tests, including horizontal bidirectional loading tests, of the proposed isolator were conducted using reduced models.

In addition, an analytical model was formulated and validated based on the test results. These experimental and analytical results are described in the following.

2 LEAD RUBBER BEARING SYSTEM WITH FAIL-SAFE MECHANISM

The authors have proposed a seismic isolation system with a sliding mechanism that maintains the

deformation of a rubber bearing within a certain allowable value. The system consists of a rubber bearing with damping capability, such as an LRB or high damping rubber (HDR) bearing, and a sliding bearing with a high friction coefficient. The two bearings are connected in series. In this study, an LRB was used as the rubber bearing. The system functions as a conventional LRB during earthquakes smaller than DBE. The sliding bearing slides under earthquakes larger than DBE, preventing the failure of the LRB as well as the excessive deformation of the building.

This system is similar to a conventional elastic sliding bearing (Hibino et al. 2012) and to the isolator that was used in the Koeberg nuclear power plant (Guéraud et al. 1985). The isolator in Koeberg was a combination of a chloroprene rubber bearing and sliding bearing. The proposed system differs from these isolators in that it uses a rubber bearing with damping capability and a fail-safe of a sliding bearing in order to prevent the failure of the rubber bearing.

3 DYNAMIC LOADING TESTS

Yamamoto et al. (2012b) reported that shear strain developed under torsional deformation caused by horizontal bidirectional loading of an HDR bearing, and that the local shear strain was increased under bidirectional loading compared to that formed under unidirectional loading. This behaviour is caused by the damping force of the isolator. The proposed system also generates a damping force; therefore, horizontal bidirectional loading tests were conducted for reduced-size specimens to clarify the bidirectional characteristics of the proposed system.

3.1 Test Specimen

The real sizes of the system are 900 × 900 mm and 1500 × 1500 mm. The specimens were both reduced to 200 × 200 mm in size, as shown in Table 1. Specifications of the test specimen are shown in Figure 1. While only one LRB for each size was used in all tests, four sets of the slider part (polytetrafluoroethylene (PTFE) plates and stainless steel sliding plate) for each LRB, eight sets in total, were placed and replaced for every vertical pressure condition.

Table 1. Specifications of test specimens

Items			Specimen No.1	Specimen No.2
Nominal size		mm	200 (900)*	200 (1500) *
LRB	Thickness of rubber sheet	mm	1.29 (5.8) *	0.93 (7.0) *
	Number of rubber sheets		34 (34) *	29 (29) *
	Thickness of inner steel plate	mm	1.2 (4.3) *	1.2 (4.3) *
	Number of lead plugs		1 (4) *	1 (4) *
Slider	Total area	mm^2	38,350 (755,500) *	38,350 (2,114,000) *

* Value in round brackets indicates that for corresponding assumed full-size bearing.

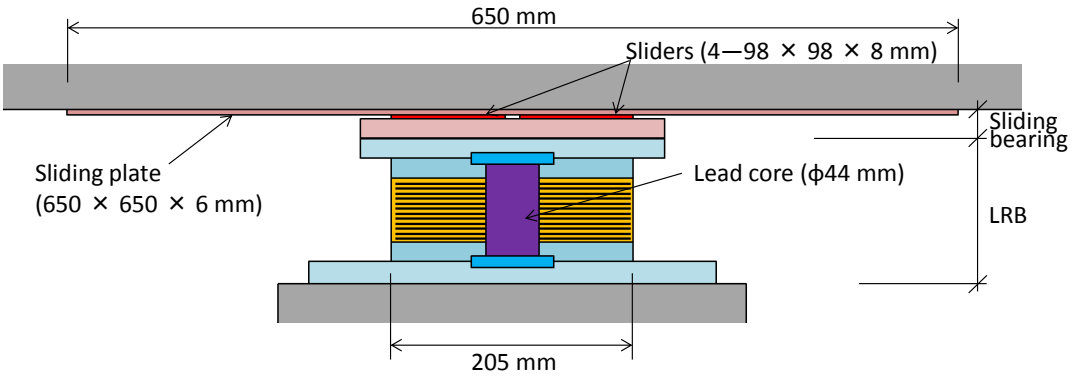

Figure 1 - Section of test specimen.

3.2 **Input Excitation**

Tests were conducted using a three-axis testing machine (Yamamoto et al. 2012a). Test parameters were the horizontal loading orbit (Figure 2), vertical pressure (Figure 3) on the slider, and loading frequency. Test cases are listed in Table 2 according to these parameters. A break-in loading was conducted after replacing the slider part before starting the test series in Table 2.

Table 2. Test cases

Test case*	Vertical pressure** (MPa)	Horizontal orbit	Frequency (Hz)	Maximum velocity (mm/s)	Maximum displacement (mm)	Repeated cycles
i-j-01 / i-j-02	4, 8, 12, var	Unidirectional	0.02 / 0.2	25.1 / 251	200.0 (0.0)***	4
i-j-03 / i-j-04		4:1 ellipse		24.4 / 244	194.0 (48.5)***	
i-j-05 / i-j-06		2:1 ellipse		22.5 / 225	178.9 (89.4)***	
i-j-07 / i-j-08		Circle		17.8 / 178	141.4 (141.4)***	
i-j-09 / i-j-10		Unidirectional		25.1 / 251	200.0 (0.0)***	

* i (= 1, 2) represents specimen No.; j (= 4, 8, 12, var) represents vertical pressure.
** Condition 'var' varies vertical pressure according to major axis displacement, as shown in Figure 3.
*** Values in round brackets indicate maximum displacement in the minor axis.

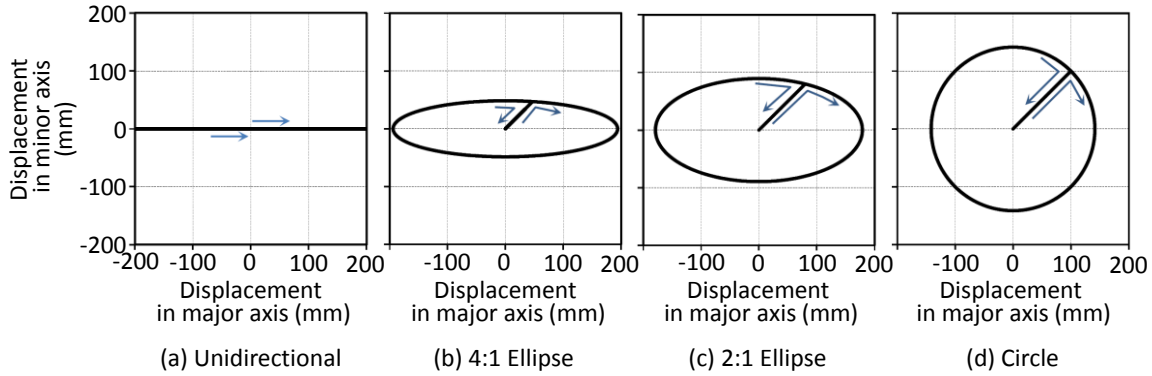

Figure 2 - Horizontal loading orbits.

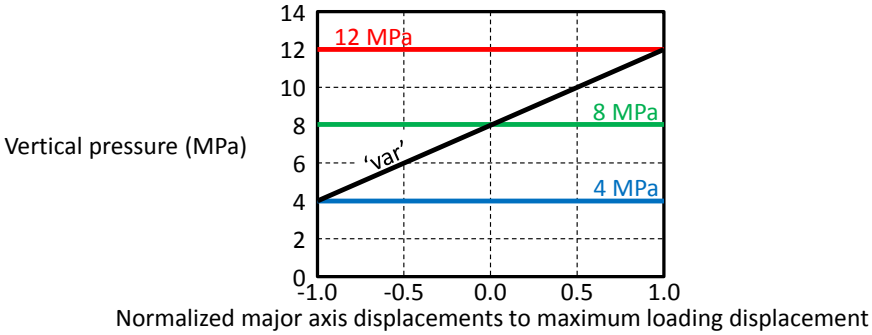

Figure 3 - Vertical pressure patterns.

3.3 **Measured Items**

The actuator displacements and six force components measured by load cells were provided by the testing machine. In addition to these measurements, potentiometer-type displacement transducers were installed to measure the deformation of the rubber part directly. By using four displacement transducers, torsional deformations as well as two horizontal deformations were obtained (Yamamoto et al. 2012a; Kamoshita et al. 2014). A thermocouple was installed at the centre of the sliding plate from the rear side.

3.4 **Evaluation Methods**

3.4.1 *Sliding Velocity, Vertical Pressure, and Friction Coefficient*

Hereafter, subscripts of *x*, *y*, and *z* indicate that the values correspond to the major, minor, and vertical axes, respectively.

Sliding velocity was estimated at the centre of the slider surface to the sliding plate. Vertical pressure was the vertical force, F_z, measured by the load cell divided by the slider surface area, A_s. The friction coefficient μ was estimated as the horizontal force, $\boldsymbol{F} = (F_x, F_y)$, measured by the load cell and divided by F_z, and as a compensated value at 20 °C (Hamaguchi et al. 2013).

Representative values for each test case were evaluated as the average values of the measured items at the time when the displacement in the major axis of slider part was changed from positive to negative, and later from negative to positive. It is noted that the loading began as a positive displacement for all cases.

3.4.2 *Shear Strain of LRB*

A torsional deformation formed from a moment in the vertical axis, generated according to the horizontal bidirectional loading. The average shear strain induced by torsional deformation at the corner of the LRB, γ_{tor_ave}, is estimated using the observed torsional angle θ:

$$\gamma_{tor\_ave} = (\theta d / 2) / h \tag{1}$$

where *d* and *h* are the diagonal length and total rubber thickness, respectively, of the LRB.

Considering the equilibrium of forces shown in Figure 4(a), and assuming the distribution of moment and shear strain as Figure 4(b), the shear strains, γ_{tor_fix} and γ_{tor_slider}, at the fixed and sliding ends of the LRB at the corner are given by the following equations (Kamoshita et al. 2014):

$$\gamma_{tor\_fix} = \gamma_{tor\_ave} + \gamma_{tor\_dif} \tag{2}$$

$$\gamma_{tor\_slider} = \gamma_{tor\_ave} - \gamma_{tor\_dif} \tag{3}$$

$$\gamma_{tor\_dif} = (F_x \delta_y - F_y \delta_x) d / (4GI_p) \tag{4}$$

where *G* and I_p are the shear modulus and polar modulus, respectively, of the LRB.

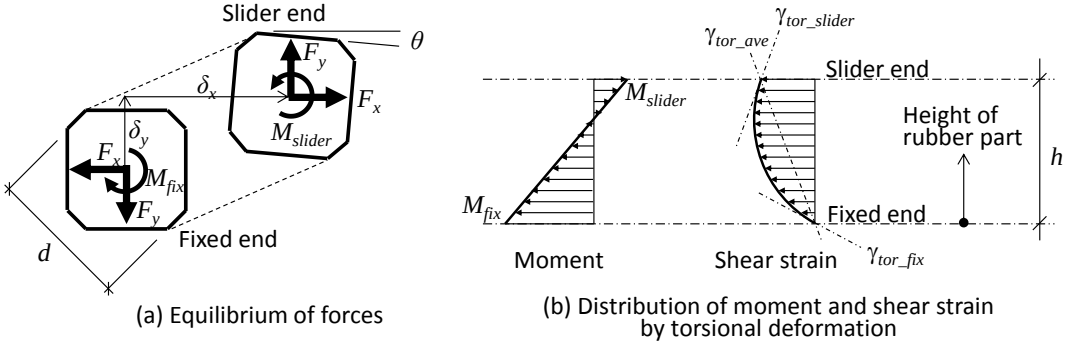

Figure 4 - Assumed conditions.

3.5 **Test Results**

3.5.1 *Friction Characteristics of Slider Bearing*

The initial friction coefficients for test cases No.i-j-01 and 02, and the rates of change of the final friction coefficients for the test cases No.i-j-09 and 10 to the corresponding initial friction coefficient are summarized in Table 3. In the case of *j* = 'var', conducted under variable vertical pressure, the coefficient is estimated when the vertical pressure is 8 MPa. The change of the friction coefficient is

not significant even after experiencing various bidirectional loadings.

Figure 5 shows a comparison of the friction coefficients under various loading patterns from test cases No.i-j-01–08 (i = 1, 2; j = 4, 8, 12). The following design equation of the friction coefficient (Hamaguchi et al. 2013) at 20 °C is also plotted in the figure:

$$\mu(\sigma_s, V_s) = 0.32\sigma_s^{-0.42} - 0.0874\sigma_s^{-1.087}\ln(160/V_s) \quad \text{for } V_s < 160$$

$$\mu(\sigma_s, V_s) = 0.32\sigma_s^{-0.42} \quad \text{for } V_s \geq 160 \qquad (5)$$

where V_s is the velocity of the slider part with units of mm/s. The unit of the vertical pressure σ_s is MPa. The friction coefficients are almost equal under every loading pattern for both specimens, and agree well with equation (5).

Table 3. Initial friction coefficients and change rates from initial to final

Vertical pressure (MPa)	Frequency (Hz)	Specimen No.1		Specimen No.2	
		Initial Coefficient	Change rate	Initial Coefficient	Change rate
4	0.02	0.146	−4.4%	0.145	−11.1%
	0.2	0.188	+0.6%	0.182	−1.6%
8	0.02	0.123	+5.4%	0.119	−6.6%
	0.2	0.142	+1.7%	0.138	+7.4%
12	0.02	0.100	−11.0%	0.109	−4.7%
	0.2	0.104	−9.6%	0.118	+5.0%
var	0.02	0.115	+2.9%	0.120	−3.3%
	0.2	0.130	−0.4%	0.140	+7.6%

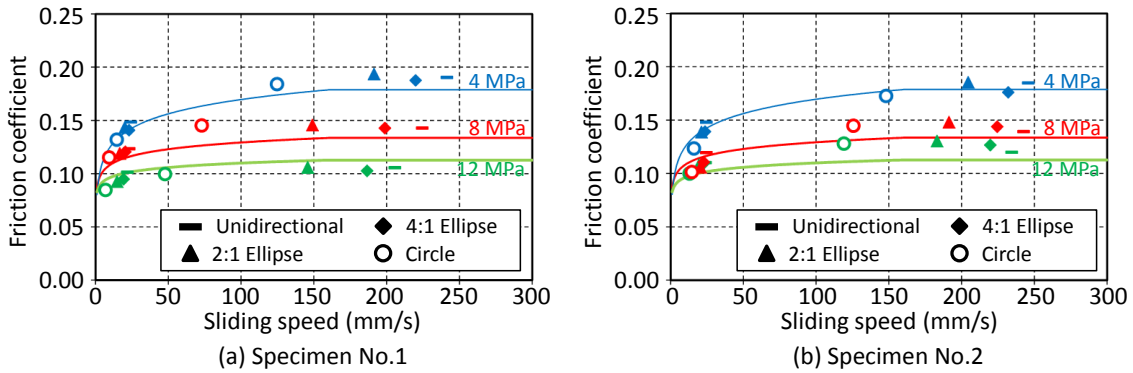

Figure 5 - Comparison of friction coefficients.

3.5.2 *Shear Strain in LRB*

The maximum shear strains of LRB, γ_{centre}, γ_{tor_fix}, and γ_{fix} under various loading patterns and vertical pressures are summarized in Table 4. The value γ_{centre} indicates the shear strain at the centre of the LRB, which does not include strain due to torsional deformation. The value γ_{fix} is the summation of γ_{centre} and γ_{tor_fix}; however, the maximum values of γ_{fix} were estimated in the time domain, and hence did not match the summation of the maxima of γ_{fix} and γ_{centre}. The results for specimen No.2 at 0.2 Hz (No.2-j-02, 04, 06, 08) are used in the table, because the results are almost the same between specimens Nos. 1 and 2, and at the frequencies 0.02 and 0.2 Hz.

Bidirectional loading also increased γ_{centre} from that measured under unidirectional loading, as Yamamoto et al. (2012a) reported for a conventional elastic sliding bearing. The ratio of γ_{fix} under bidirectional loading to that under unidirectional loading is calculated and listed in Table 4. The ratio is reduced with the vertical pressure.

Photographs of the deformed LRB and the time-histories of γ_{centre}, γ_{tor_fix}, and γ_{fix} are shown in Figure 6. For horizontal biaxial loading of circular shape under the vertical pressure of 4 MPa (Figure 6(b)), a large torsional deformation of the rubber is observed in the slider end of the LRB. In this case, the fixation degree of the slider end seems to be small. However, for loading under the vertical pressure of 12 MPa (Figure 6(d)), the fixation degree of the slider end seems sufficiently high to constrain the torsional deformation at the end.

Table 4. Shear strains

Loading pattern*	Vertical pressure (MPa)	γ_{centre}	γ_{tor_fix}	γ_{fix}	Increase**	Vertical pressure (MPa)	γ_{centre}	γ_{tor_fix}	γ_{fix}	Increase**
Uni	4	1.02	0.15	1.15	—	12	2.94	0.22	3.00	—
4:1		1.39	0.66	2.00	+73.8%		3.09	0.31	3.26	+8.7%
2:1		1.53	0.92	2.35	+104.4%		3.03	0.29	3.30	+9.8%
Circle		1.51	1.06	2.40	+108.5%		3.15	0.27	3.32	+10.5%
Uni	8	2.19	0.28	2.36	—	var	2.77	0.11	2.80	—
4:1		2.45	0.41	2.57	+8.9%		3.09	0.49	3.23	+15.2%
2:1		2.47	0.42	2.71	+14.8%		3.12	0.54	3.30	+17.7%
Circle		2.61	0.52	2.88	+22.0%		3.21	0.53	3.38	+20.4%

* Uni: Unidirectional; 4:1: 4:1 Ellipse; 2:1: 2:1 Ellipse.
** Increase ratio of γ_{fix} under bidirectional loading to unidirectional loading.

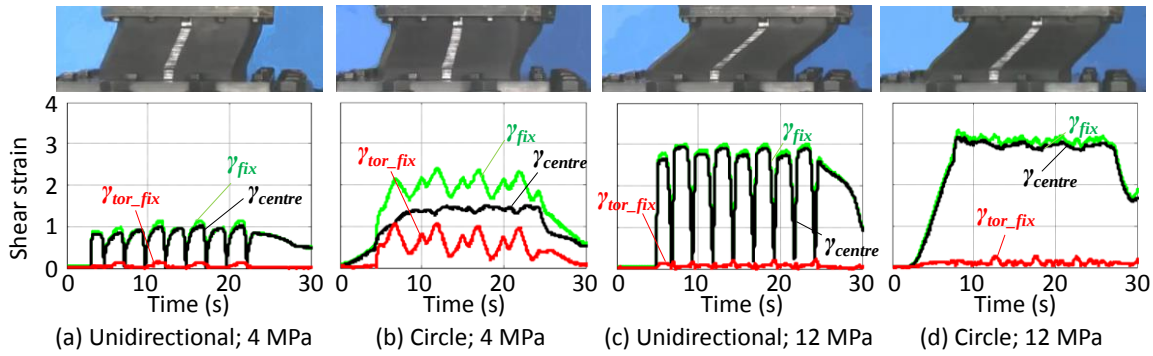

Figure 6 - Photographs of deformed LRB and time-histories of shear strains.

4 SIMULATION ANALYSIS

4.1 Analytical Model

An analytical mechanical model of the proposed bearing was developed by modifying the model for an elastic sliding bearing presented by Kamoshita et al. (2014). The proposed bearing model must include the elasto-plastic behaviour of LRB, which was not considered in the previous model. Figure 7 shows an illustration of the developed model.

This model has three nodes, which are representative of the fixed-end flange plate of the LRB (point P), the slider (point Q), and the sliding plate (point O). Horizontal restoring force characteristics of the LRB were implemented between points P and Q. The LRB, which was implemented between points P and Q, was modelled as a multiple shear springs (MSS) model in which the elemental springs were modelled by the Kikuchi-Aiken model, as in Nakamura et al. (2012). The sliding bearing, implemented between points Q and O, was modelled as a bidirectional friction element constituted by equation (5).

The friction element and the LRB model affect each other intricately. In order to address this, the

following equation was introduced. By iterating using the equation, the parameter α and then the incremental displacements of the friction element Δq_x and Δq_y are obtained:

$$\begin{Bmatrix} \Delta q_x \\ \Delta q_y \end{Bmatrix} = \alpha \left(\beta \begin{Bmatrix} d_x \\ d_y \end{Bmatrix} + (1-\beta) \begin{Bmatrix} f_x / k_x \\ f_y / k_y \end{Bmatrix} \right) \tag{6}$$

where d, f, and k denote the deformation, force, and stiffness of the LRB model, respectively. The parameter β was set as 0.5 in this study.

The above analytical mechanical model was implemented in the OpenSees software program (Open System for Earthquake Engineering Simulation; http://opensees.berkeley.edu).

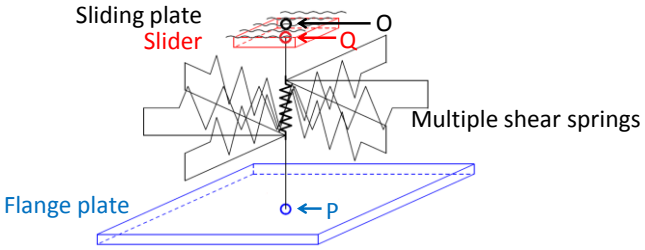

Figure 7 - Analytical mechanical model.

4.1. Simulation Results

In the following, the test results from specimen No.2 were used for comparison. Figure 8(a) shows the simulation results for the force–displacement relationship in the test cases under the constant vertical pressure of 8 MPa (No.2-08-01, 02, 05, 06). Figure 8(b) shows the results for the test cases under varied vertical pressure (No.2-var-01, 02, 05, 06). Considering the effects of repeated loadings on the specimen, the second stiffness and yield strength of the LRB model were adjusted by multiplying 1.0 and 1.3 times for the 8-MPa pressure test cases, and by 0.8 and 1.2 times for the varied-pressure test cases, respectively. The proposed model simulates the force–displacement relationships well for both unidirectional and bidirectional loading, for both constant 8 MPa and varied pressure, and for frequencies of both 0.02 and 0.2 Hz.

5 CONCLUSIONS

A seismic isolation system with a high safety margin for large earthquakes that exceed DBE was proposed in this paper. This system consists of a LRB and a sliding bearing with a high friction coefficient connected in series. Dynamic loading tests were conducted using reduced-size specimens of 200 × 200 mm. The results showed that the friction characteristics were almost equal among all tested loading patterns and agreed well with a design equation identified based on previous unidirectional loading test results. However, local shear strains were increased by bidirectional loading. This increased shear strain tendency was dominant when the vertical pressure was small.

An analytical model of the proposed isolation system was developed. Simulation analysis results showed that the developed model simulated the force–displacement relationship of the system well for both unidirectional and bidirectional loadings, even under varied vertical pressures.

6 ACKNOWLEDGEMENTS

This research was partially supported by the Japan Society for the Promotion of Science, Grant-in-Aid for Scientific Research (A), 15H02274, 2016. The authors would like to express their thanks to those organizations. Dynamic loading tests in this paper were conducted at the Oiles Corporation, Japan. The authors would like to express their thanks to Mr. Nagata, Dr. Kouchiyama, and Dr. Nakamura of the Oiles Corporation for their advices on the tests. The authors would like to also express their thanks to Dr. McKenna of the University of California, Berkeley, for his advice on the development of the simulation model.

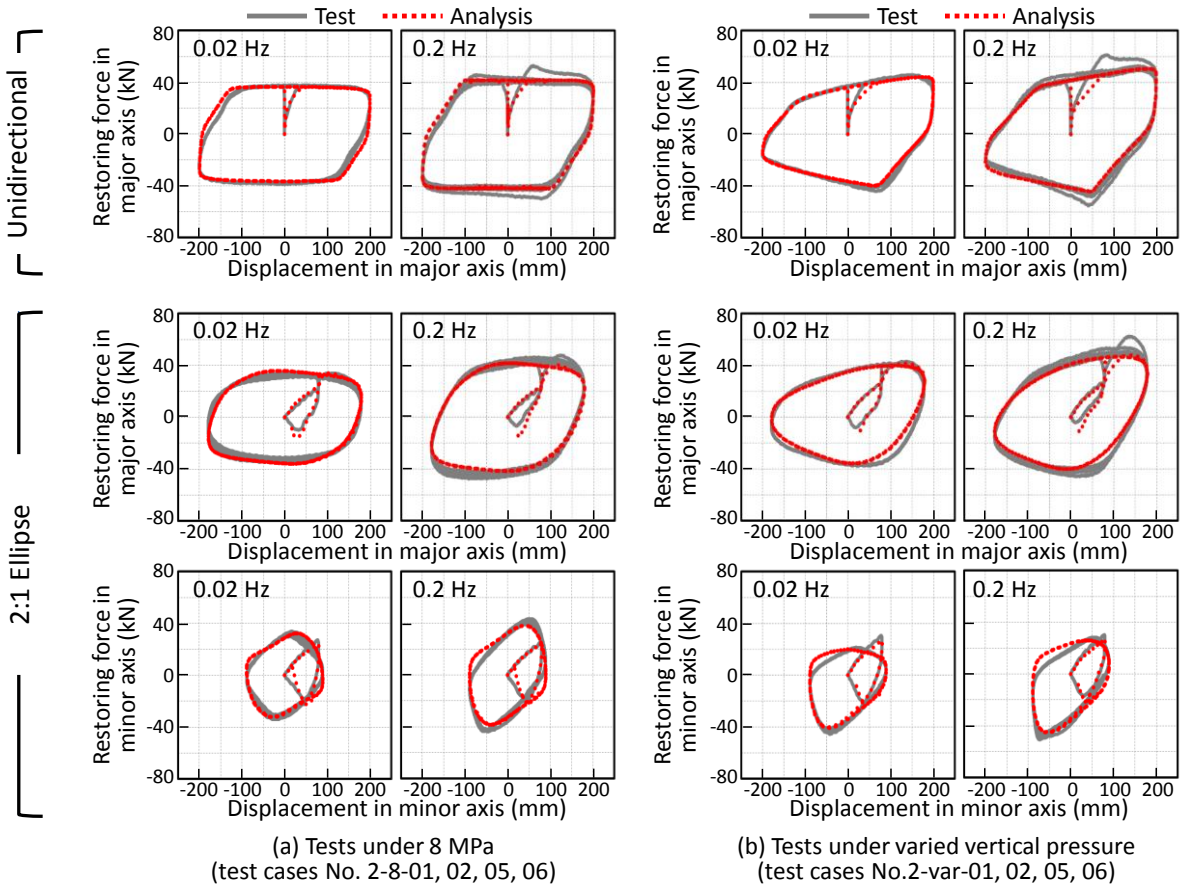

Figure 8 - Simulation results.

REFERENCES

Guéraud, R. Noël-Leroux, J.P., Livolant, M. & Michalopoulos, A. P. 1985: Seismic isolation using sliding-elastomer bearing pads, *Nuc. Eng. and Des.*, 84(3):363-377.

Hamaguchi, H., Yamamoto, M., Higashino, M. & Taniguchi, H. 2010. A proposal of a seismic isolation system with high safety margin for unexpected input ground motions (part 1) Outline, *Summ. Tech. Pap. Annu. Meet., AIJ*, B2:437-438 (in Japanese).

Hamaguchi, H., Yamamoto, M., Wake, T. & Miyazaki, M. 2013. A proposal of a seismic isolation system with high safety margin for unexpected input ground motions (part 8) Evaluation of the dynamic friction factor of a suggesting bearing, *Summ. Tech. Pap. Annu. Meet., AIJ*, B2:803-804 (in Japanese).

Hibino, H., Maseki, R., Nii, A., Minewaki, S., Yamamoto, M., Yoneda, H., Takayama, M., Kikuchi, M. & Iiba, M. 2012. Safety verification of seismic isolation system using sliding bearings against long period earthquake motions, *15th World Conf. Earthq. Eng., Lisbon, Portugal*.

Kamoshita, N., Yamamoto, M., Minewaki, S., Kikuchi, M., Ishii, K., Kouchiyama, O. & Nakamura, T. 2014. Horizontal bidirectional characteristics of elastic sliding bearings under various fluctuant vertical loading conditions, *J. Struct. Constr. Eng. AIJ*, 79:453-464 (in Japanese).

Nakamura, T., Kikuchi, M., Ishii, K. & Kouchiyama, O. 2012. Hysteresis properties of lead rubber bearings under horizontal bi-directional deformation, *J. Struct. Constr. Eng. AIJ*, 77:1663-1671 (in Japanese).

Yamamoto, M., Minewaki, S., Kamoshita, N., Kikuchi, M., Ishii, K., Kouchiyama, O. & Nakamura, T. 2012a. Behaviors of a sliding rubber bearing under horizontal bidirectional loadings, *15th World Conf. Earthq. Eng., Lisbon, Portugal*.

Yamamoto M., Minewaki S., Yoneda, H. & Higashino, M. 2012b. Nonlinear behavior of high-damping rubber bearings under horizontal bi-directional loading: Full-scale tests and analytical modelling, *Earthq. Eng. Struct. Dyn.*, 41:1845-1860.